Unified band-theoretic description of structural, electronic, and magnetic properties of vanadium dioxide phases

Sheng Xu, Xiao Shen, Kent A. Hallman, Richard F. Haglund, Jr., and Sokrates T. Pantelides

Phys. Rev. B **95**, 125105 — Published 6 March 2017

DOI: 10.1103/PhysRevB.95.125105

Unified band-theoretic description of structural, electronic, and magnetic properties of vanadium dioxide phases

Sheng Xu,[1,2] Xiao Shen,[2,3] Kent A. Hallman,[2] Richard F. Haglund, Jr.,[2]

Sokrates T. Pantelides[2,4]

[1] *School of Metallurgy and Materials Engineering, Jiangsu University of Science and Technology, Zhangjiagang, Jiangsu 215600, China*

[2] *Department of Physics and Astronomy, Vanderbilt University, Nashville, TN 37235-1807, USA*

[3] *Department of Physics and Materials Science, University of Memphis, Memphis, TN 38152, USA*

[4] *Department of Electrical Engineering and Computer Science, Vanderbilt University, Nashville, TN 37235-1807, USA*

(Received 30 January 2017)

The debate about whether the insulating phases of vanadium dioxide (VO_2) can be described by band theory or must invoke a theory of strong electron correlations remains unresolved even after decades of research. Energy-band calculations using hybrid exchange functionals or including self-energy corrections account for the insulating or metallic nature of different phases, but have not yet successfully accounted for the observed magnetic orderings. Strongly-correlated theories have had limited quantitative success. Here we report that, by using hard pseudopotentials and an optimized hybrid exchange functional, the energy gaps and magnetic orderings of both monoclinic VO_2 phases and the metallic nature of the high-temperature rutile phase are consistent with available experimental data, obviating an explicit role for strong correlations. We also found a potential candidate for the newly-found metallic monoclinic phase.

PACS numbers: 71.27.+a, 75.30.-m, 71.20.-b

I. INTRODUCTION

Vanadium dioxide (VO_2) exhibits a first-order phase transition from an insulating phase to a metallic phase at 340 K [1], which is accompanied by a structural transition from the monoclinic M1 phase to the tetragonal rutile (R) phase. VO_2 is intensively studied for such applications as temperature-tuned memory materials [2] and smart windows [3], and for optoelectronic devices [4]. It is also widely viewed as a model system for understanding insulator-to-metal transitions in solids [5–8] . The M1 phase of VO_2 has a band gap of 0.6-0.7 eV [9,10] and can be considered nonmagnetic (NM) [11] near room temperature, while the metallic R phase is

paramagnetic (PM) [9,12] above the transition temperature. In addition to these two phases, the experimentally derived phase diagram of VO_2 [13,14] includes a second insulating monoclinic phase designated as M2, which can be stabilized in doped or strained VO_2 single crystals [15,16], thin films [17,18], and nanobeams [19]. Recently, stable metallic monoclinic (mM) phases were found near room temperature under high pressure [20] and in thin films [21,22]. These phases may be related to the transient metallic monoclinic state already reported in ultrafast experiments [23,24].

The theoretical description of VO_2 phases has been controversial for half a century. The debate has centered on whether the insulating phases can be described by single-quasiparticle band theory or the band gap results from strong correlations in the Mott-Hubbard sense [15,16,25,26]. In 1971, Goodenough suggested that the band gap in VO_2 can originate from the formation of V-V pairs [27], but, in 1975, Zylbersztejn and Mott proposed that the band gap in VO_2 originates largely from strong electron correlations [28]. This thesis subsequently gained support from experimental data that showed behavior similar to the generic, non-material-specific predictions of correlated-electron model Hamiltonians [25,29]. In 1994, density-functional theory (DFT) calculations for the M1 phase, based on the local density approximation (LDA) for the exchange-correlation potential, favored a Peierls-like dimerization of V atoms as the root of insulating behavior [30]. However, these DFT calculations did not yield a true band gap, a failure which strengthened arguments for a Mott-Hubbard description of the band gap [29,31]. In 2005, Biermann *et al.* carried out dynamical mean-field theory (DMFT) calculations, effectively building electron correlations into DFT-LDA calculations that give zero energy gap [32]. They found a nonzero band gap for the M1 phase, but concluded that M1 *is not a conventional Mott insulator*; instead, the finite band gap was attributed to a *correlation-assisted Peierls transition*. The role of strong correlations in opening the band gap was further corroborated in more recent calculations by Weber et al. [33].

In the last decade, single-particle theories have been extensively explored and tested against experimental data. In 2007, Gatti *et al.* [34] calculated VO_2 energy bands using Hedin's GW approximation for the one-electron Green's function [35], which replaces the bare Coulomb potential in the Hartree-Fock (HF) approximation by an energy-dependent screened Coulomb interaction. These calculations produced an energy gap in the M1 phase and a metallic rutile phase. In 2011, Eyert [36] reported energy-band calculations using hybrid exchange-correlation functionals, in which a fraction of the local exchange potential is replaced by HF exchange. He obtained satisfactory energy gaps for the insulating phases, duplicating the success of Gatti *et al.* [34], and addressed the issue of magnetic ordering. While this initial success was followed by more comprehensive studies [37–39], no single exchange-correlation functional has been found that reproduces both the observed energy gaps and magnetic orderings of VO_2 phases, so that the applicability of band theory to VO_2 remains in dispute. Furthermore, fixed-node diffusion quantum Monte Carlo calculations, which do not depend on a choice of functional, also predicted the proper band gaps without reproducing the observed magnetic ordering [40].

In this Letter, we introduce two novel elements in energy-band calculations for the principal

phases of VO_2: (1) significantly harder pseudopotentials for both oxygen and vanadium and (2) an optimized mixing parameter in a hybrid functional for the exchange-correlation potential. The calculated lattice constants, band gaps, and magnetic properties of the R, M1 and M2 phases of VO_2 are consistent with available experimental data. Additionally, the calculated density of states (DOS) for the M1 and R phase are quantitatively consistent with experimental x-ray photoemission (XPS) data. The success of these hybrid DFT calculations demonstrates that band theory can describe VO_2 phases without explicitly invoking strong correlations. Moreover, the calculations predict a new monoclinic phase with a crystal structure intermediate between M1 and R, which we call the M0 state. The M0 phase is ferromagnetic and the true ground state of VO_2 at absolute zero. Old data at liquid-helium temperature [41,42] suggest the existence of such a phase at near-zero temperatures, but more comprehensive data are needed to confirm the prediction. M0 may also be a candidate for the recently discovered [20–22] metallic monoclinic (mM) phase of VO_2 at finite temperatures.

II. COMPUTATIONAL DETAILS

Hybrid DFT calculations for each VO_2 phase were performed using a plane-wave basis and the projector-augmented-wave method [43] as implemented in the Vienna Ab initio Simulation Package (VASP) [44]. Several magnetic configurations were calculated to determine the magnetic ordering for each VO_2 phase. The exchange and correlation were described by a tuned PBE0 hybrid functional [45,46] that contains 7% HF exchange, which yields an energy gap for M1 in agreement with experiment. These calculations provide a more accurate description of the vanadium and oxygen atoms for two reasons. Firstly, thirteen electrons ($3s^2 3p^6 3d^4 4s^1$) were treated as valence electrons for vanadium instead of the typical eleven electrons [36,38]. For the oxygen atoms, six electrons ($2s^2 2p^4$) were treated as valence electrons as usual. Second, the oxygen pseudopotential in these calculations was harder than typically used (i.e., the core radius is smaller). The AFM-M1 phase is metastable using typical oxygen pseudopotentials but is unstable using a hard potential, which reflects a delicate balance between competing effects, as manifest by a complex phase diagram with multiple competing phase transitions. The hardness of pseudopotential has an effect on the magnetic order because it affects bond lengths (and/or bond angles) and this indirectly affects whether a certain magnetic order can be stabilized or not, which is known as the Goodenough-Kanamori rule [47–49].

Such materials may also require a description using hard pseudopotentials. As required by the harder oxygen pseudopotential, the plane-wave cutoff energy was set at 700 eV; a cutoff energy of 800 eV caused no appreciable changes. All Brillouin-zone sampling was based on Γ-centered k-point grids. We used 3×3×3 grids for the M1 and M0 unit cells that each contain 12 atoms, a 4×4×6 grid for the R unit cell with 6 atoms, and a 1×2×2 grid for the M2 unit cell with 24 atoms. The self-consistent electronic calculations were converged to 10^{-4} eV between successive iterations and the structural relaxations were converged so that the total-energy difference between two successive ionic steps is 10^{-3} eV. The initial magnetic configuration was set by assigning a moment of 0, +1, or -1 Bohr magneton on each vanadium atom, resulting in three possible initial configurations: NM (all moments set at 0), FM (all moments set at +1), and AFM (moments alternating between +1 and -1 along V-chains). During self-consistency

calculations of the electronic structure, the magnetic moments on all atoms were allowed to vary.

III. RESULTS

The optimized crystal structures in Figure 1 have all expected features of the experimentally-derived structures: all V-V chains of M1 and M0 are both canted and dimerized, R has only undimerized straight V-V chains, and the monoclinic M2 phase has both straight dimerized V-V chains and undimerized but canted antiferromagnetic V-V chains [16,22,50–52]. In addition to that qualitative agreement, the calculated lattice constants and angles as well as vanadium-vanadium (V-V) bond lengths and V-V angles are in good agreement with corresponding experimental values (see Table I). Although our lattice constants and V-V bond lengths are somewhat smaller than the corresponding experimental values, density functional theory calculations simulate atoms at 0 K, not the finite temperatures available to experiments.

First, we consider the magnetic and electronic properties of the R phase. Experiments have shown that the R phase is PM above the transition temperature of 340 K [9,12]. According to the present calculations, the total energies of antiferromagnetic R (AFM-R) and NM-R are higher than ferromagnetic R (FM-R) by 125 and 140 meV per formula unit, respectively. Although the calculations predict FM-R to be the ground state of R, the temperature at which DFT calculation must be performed (0 K) is well below any hypothetical Curie temperature of R-VO_2. However, the crystal structure of VO_2 is monoclinic at temperatures below 340 K so we cannot directly compare the calculated FM ground state to an experimentally-observed state, so we can only state that our FM-R prediction is consistent with the experimental observations of PM-R [9,12]. As shown in Table II, FM-R is metallic, in agreement with experiment [9,12], DMFT calculations [32], and a previous hybrid-functional calculation [53], but unlike other hybrid calculations [38,54]. In Figure 2(a), the total DOS of FM-R is compared to the experimental XPS spectra [55] and with DMFT results [32]. The overall shape of the DOS agrees with the experimental data. In particular, a feature at -1.3 eV that is present in the experimental data [55], in previous DMFT results (attributed to a lower Hubbard band) [32], and in GW calculations (attributed to a plasmon) [34] is reproduced in the DOS computed in the present work.

We next consider the magnetic and electronic properties of the M1 phase. Conflicting reports of paramagnetic [9,12] and diamagnetic [56] susceptibilities for M1 suggest that M1 probably has a negligible magnetic susceptibility, and that experimental values are potentially affected by fabrication parameters; we therefore designate it as NM as previous authors have done [38]. The optimized AFM-M1 spin configuration relaxes to the more stable NM-M1 in contrast to previous hybrid DFT results [36–38,53] but consistent with experiment [9,11,12]. As can be seen in Table II, we obtain a band gap of 0.63 eV for NM-M1 in good agreement with the experimental value [9,10,55] of 0.6-0.7 eV and the values obtained from DMFT [32,33] and GW [34] calculations. In Figure 2, the total DOS of NM-M1 is compared to the experimental XPS spectra [55] and the GW DOS of Ref. [34]. The shape of the DOS and the positions of peaks from -10 to 0 eV agree well with the experimental results [55] and with the GW DOS. This comparison confirms that the electronic structure of the insulator phase NM-M1 is correctly reproduced by the present hybrid DFT calculations.

In addition to the NM-M1 and FM-R states, the present hybrid DFT calculations predict a stable ferromagnetic state, FM-M0, with a structure intermediate between NM-M1 and FM-R. Calculations starting from the FM-M1 configuration converge to FM-M0 during geometry optimization. Since the total energy of FM-M0 is lower than the calculated energy of the commonly accepted ground state, NM-M1, by ~50 meV per formula unit, we suggest that VO_2 may be ferromagnetic at very low temperatures. A low Curie temperature could account for the discrepancy between the predicted ferromagnetism and the finite magnetic susceptibility observed in experiments at moderately low temperatures [41,42]. Between 10 K and the insulator-to-metal transition at ~340K the magnetic susceptibility is small [42], reinforcing the conventional wisdom that NM-M1 is the stable phase above 10 K.

It is noteworthy that initial configurations of AFM-M0 and NM-M0 both converge to NM-M1 when the initial magnetic moments are allowed to change during the calculation. Along with the fact that FM-M1 converges to FM-M0, these calculations hint at the complex interplay of magnetic and structural degrees of freedom, and highlight the necessity of more magnetic measurements at low temperatures to confirm previous experimental results [41,42] and our theoretical predictions. In other words, the input magnetic ordering of (FM or NM) is a stronger determinant of the output crystallographic structure (M0 or M1, respectively) than the input crystallographic structure. It is also interesting that our results show that both ferromagnetic phases of VO_2 (M0 and R) are half metals, as is CrO_2 [57,58], suggesting that half metallicity and ferromagnetism are correlated in transition-metal oxides.

Similar to NM-M1, the FM-M0 configuration has a simple monoclinic lattice with space group P21/c (C^5_{2h}, No. 14) and dimerized zigzag V-V chains. However, the crystal structures of NM-M1 and FM-M0 exhibit subtle differences, as shown in Figures 1(a) and 1(b). The short V-V bond of FM-M0 is longer and the long bond is shorter than the corresponding bonds in NM-M1. Therefore, the FM-M0 crystal structure can be viewed as an intermediate state between the crystal structures of NM-M1 and FM-R. In fact, both the short and long V-V bonds of FM-M0 are closer to the bond length found in FM-R than their NM-M1 counterparts, indicating a FM-M0 intermediate state would be structurally closer to FM-R than to NM-M1. Furthermore, the 175° bond angle of FM-M0 is also closer to the 180° angle found in FM-R than the 166° angle of NM-M1. Diffraction measurements and optical or electrical measurements below the Curie temperature are needed to verify the structure and metallic character of the FM-M0 state.

Recently, a stable metallic monoclinic VO_2 phase (mM) has been observed near room temperature in thin films [22] and single crystals under high pressure [20]. We found that the crystal structures and metallic character of the predicted FM-M0 and the experimental mM states are very similar, which suggest that FM-M0 may be related to this mM phase. In the thin films [22], X-ray absorption fine-structure spectroscopy (XAFS) demonstrated that the short V-V bond elongates, the long V-V bond shortens, and zigzag V-V chains straighten when VO_2 metallizes [22], leading to an intermediate crystal structure with lattice constants and bond lengths nearly identical with those for FM-M0 shown in Table I. Pressure-dependent Raman spectroscopy, mid-infrared reflectivity, and optical conductivity measurements confirmed an

insulator-to-metal transition without an accompanying structural transition from monoclinic to the rutile phase [20]. However, although a subtle change in structure was attributed to the appearance of the M2 phase, that assignment explains neither the metallization nor the fact that intermediate Raman spectra are unlike those of either M2 or M1 [20]. Instead, a monoclinic metallic phase, such as M0, with slightly different crystal structure than either M1 or M2, would explain both the mM phase in thin film samples [22] and the metallic monoclinic VO_2 phase that appears under high pressure [20]. The similar crystal structures and metallic character of the predicted FM-M0 and the experimental mM states suggest that FM-M0 may be related to this mM phase.

Although most work on VO_2 over the past fifty years has focused exclusively on the transition between the insulating M1 and metallic R phases, multiple authors [14,16,29,36,59] have suggested that the M2 insulating phase may hold the key to a complete understanding of the VO_2 phase transition. Three possible AFM configurations [60] designated as A-AFM, G-AFM, and C-AFM are shown in Figure 3(a), 3(b), and 3(c), respectively. Each configuration represents a unique magnetic ordering of the zigzag chains, while the straight chains have no moments. The A-type and G-type exhibit antiparallel moments along the canted zigzag V-V chains [16]. For A-AFM, moments on V-atoms in a canted zigzag chain are parallel to moments of its nearest V-atom neighbors on the next canted chain, while they are antiparallel for G-AFM and C-AFM. However, the moments of all vanadium atoms on a single chain are aligned in C-AFM.

Our calculations show that the A-AFM is the lowest-energy configuration of M2 and the G-AFM, C-AFM, FM, and NM configurations of M2 are higher in energy than A-AFM by 4 meV, 27 meV, 16 meV, and 32 meV per formula unit, respectively. Although numerically accurate, the small energy difference (4 meV) between A-AFM and G-AFM may not be captured accurately by the approximate functionals. Nevertheless, both A-type and G-type AFM-M2 agree with the experimentally derived model in which M2 is antiferromagnetic and local magnetic moments are present only on the canted zigzag V-V chains [16]. Similarly, the present calculations show that the local magnetic moments of AFM configurations are on the canted V-V chains while the straight, dimerized chains have negligible moments. The band gap of 0.56 eV calculated for A-AFM-M2 is in agreement with photoelectron spectroscopy (PES) of M2 quoting a band gap greater than 0.1 eV [61]. Furthermore, our value of 0.56 eV is consistent with the band model proposed by Goodenough [62] in which the band gap for M2 is comparable to, but smaller than, the band gap of M1 (0.6-0.7 eV).

IV. DISCUSSION

The kernel of the long-standing debate about VO_2 is whether the electronic properties of this material are better described by band theory in which electrons are represented by non-interacting quasiparticles that experience the same single-particle crystal potential, or by a many-body approach in which electron-electron interactions are explicitly incorporated. In principle, band theory can always describe any given material: ground-state properties are describable by DFT, which is an exact theory, assuming that a satisfactory exchange-correlation potential $V_{xc}(r)$ can be constructed; excitations can be described by Hedin's GW expansion of the

self-energy $\Sigma(r,r';E)$ followed by solving the Bethe-Salpeter equation (BSE) [63] to include electron-hole interactions. Both the DFT and Hedin equations look like Schrödinger equations: the $V_{xc}(r)$ in DFT is replaced by the nonlocal, energy-dependent $\Sigma(r,r';E)$ in order to describe excitations. Using these equations, one gets quasiparticle energy bands, single-particle excitations, excitons (via the BSE), and plasmons (from the zeros of the real part of the single-particle dielectric function [64]), but the energy dependence in $\Sigma(r,r';E)$ is often essential [33]. The standard procedure is to first solve the DFT equation with a reasonable choice of V_{xc}, and then use the solutions to construct $\Sigma(E_k)$, which are in turn used to correct the DFT energy bands. Ideally, the process should be carried to self-consistency to eliminate the effect of the initial V_{xc} choice. Gatti *et al.* [34] have already demonstrated that this process correctly predicts the band gap of insulating monoclinic VO_2, but the numerical procedures are quite cumbersome and magnetic calculations require separate, self-consistent GW calculations. Hybrid exchange-correlation functionals constitute an attempt to construct a $V_{xc}(r)$ that also serves as a local, energy-independent approximation to $\Sigma(r,r';E)$, known as the COHSEX (Coulomb hole plus screened exchange) approximation [34]. The fact that $\Sigma(r,r';E)$ is material specific justifies tuning the mixing parameter in the hybrid functional, as is done in the present paper. In this way, the tuned exchange-correlation functional models $\Sigma(r,r';E)$ *for each material.* Similarly, the Hubbard U, which is present in theories that incorporate explicit electron-electron interactions, is also often treated as a free parameter. Here we have demonstrated that, by tuning the mixing parameter of a hybrid functional and using harder-than-usual pseudopotentials, the single-particle approach correctly yields both the electronic and magnetic properties of VO_2 phases; however, the underlying nature of the phase transition is not addressed here.

DFT and GW calculations serve as rigorous *quantitative* tests of quasiparticle theories. The early conclusions that VO_2 is a strongly-correlated material were based on model many-body Hamiltonians. Experimental data in the region of the phase transition were compared with the corresponding model behavior [26,29]. The appearance of correlated behavior at the phase transition, however, does not necessarily imply that strong correlations persist at temperatures away from the phase transition. Quantitative theories based on strong correlations, such as LDA+U, GGA+U and DMFT, assume at the outset that strong electron-electron interactions, incorporated via the Hubbard-model on-site parameter U, dominate. In the case of VO_2, LDA+U yields insulating behavior for both the monoclinic and rutile phases [65,66]. The DMFT calculations by Biermann *et al.* [32] and by Weber et al. [33] are anchored on a zero-gap DFT calculation and found that strong correlations are needed to reproduce the observed value of a Peierls-induced energy gap. However, these methods have not yet been used to study the competing magnetic orderings. Thus, only the present calculations, based on band theory, reproduce the observed structural, electronic, *and* magnetic properties of all VO_2 phases. The present band theory, DMFT, and GW/COHSEX all give a band-gap value in accord with experiment, which raises the following challenge: If DMFT and GW/COHSEX calculations were to be anchored on the present hybrid-functional band structure, which yields a correct energy gap, instead of the zero-gap LDA band structure, would they retain this value of the energy gap? If so, the role of correlations beyond what is captured by the present hybrid functional would be

negligible. Clearly, such calculations would be valuable to establish the origin of the agreement between seemingly incompatible theories.

V. CONCLUSIONS

In conclusion, our study underlines the power of the hybrid DFT approach to produce a comprehensive theoretical picture of all the major VO_2 phases and their magnetic properties. We have successfully reproduced the electronic and magnetic properties of M1, M2, and R phases of VO_2 using DFT calculations with a hybrid functional and accurate pseudopotentials. The success of these hybrid DFT calculations suggests that band theory can provide an adequate description of VO_2 phases despite the unusually large coupling between magnetic and structural degrees of freedom in VO_2. The strength of that coupling is perhaps displayed more clearly in this work than ever before given the strong influence that the initial magnetic state has on the optimized crystal structure. Moreover, the present calculations predict a new monoclinic ferromagnetic metal state of VO_2, which accounts for the magnetic data at low temperature and is also a candidate for the recently observed metallic monoclinic mM phase that appears in thin films or under high pressure. In addition, the antiferromagnetic structure of M2 was predicted to be A-type. Experimental verification of ferromagnetism in room-temperature VO_2 under high pressure, as well as structural and electronic measurements at low temperatures in unstrained VO_2, clearly set important priorities for future research to test the validity of these particular findings.

ACKNOWLEDGMENTS

Computational resources were provided by the NSF XSEDE under grants TG-DMR130121, TG-DMR150028, TG-DMR150063, and by the High Performance Computing Facilities at the University of Memphis. S. Xu was supported by the Jiangsu Overseas Research & Training Program for University Prominent Young & Middle-Aged Teachers and Presidents (China). The work at Vanderbilt was funded by National Science Foundation grants DMR-1207241 (XS), DMR-1207241 (RFH), EECS-1509740 (KAH and RFH), by Department of Energy grant DE-FG02-09ER46554 (XS and STP), and by the McMinn Endowment at Vanderbilt University (KAH and STP). We thank Lucia Reining for valuable comments on the manuscript.

[1] F. J. Morin, Phys. Rev. Lett. **3**, 34 (1959).
[2] T. Driscoll, H.-T. Kim, B.-G. Chae, B.-J. Kim, Y.-W. Lee, N. M. Jokerst, S. Palit, D. R. Smith, M. Di Ventra, and D. N. Basov, Science (80-.). **325**, 1518 (2009).
[3] E. S. Lee, X. Pang, S. Hoffmann, H. Goudey, and A. Thanachareonkit, Sol. Energy Mater. Sol. Cells **116**, 14 (2013).
[4] T. S. Kasırga, D. Sun, J. H. Park, J. M. Coy, Z. Fei, X. Xu, and D. H. Cobden, Nat. Nanotech. **7**, 723 (2012).
[5] N. F. Brady, K. Appavoo, M. Seo, J. Nag, R. P. Prasankumar, R. F. Haglund, and D. J. Hilton, J. Phys. Condens. Matter 28, 125603 (2016).
[6] J. D. Budai, J. Hong, M. E. Manley, E. D. Specht, C. W. Li, J. Z. Tischler, D. L. Abernathy, A. H. Said, B. M. Leu, L. A. Boatner, R. J. McQueeney, and O. Delaire, Nature 515, 535 (2014).
[7] K. Appavoo, D. Y. Lei, Y. Sonnefraud, B. Wang, S. T. Pantelides, S. a Maier, and R. F. Haglund, Nano Lett. 12, 780 (2012).
[8] K. Appavoo, B. Wang, N. F. Brady, M. Seo, J. Nag, R. P. Prasankumar, D. J. Hilton, S. T. Pantelides, and R. F. Haglund, Nano Lett. 14, 1127 (2014).
[9] C. N. Berglund and H. J. Guggenheim, Phys. Rev. **185**, 1022 (1969).
[10] A. Cavalleri, M. Rini, H. H. W. Chong, S. Fourmaux, T. E. Glover, P. A. Heimann, J. C. Kieffer, and R. W. Schoenlein, Phys. Rev. Lett. **95**, 067405 (2005).
[11] T. Kong, M. W. Masters, S. L. Bud'ko, and P. C. Canfield, APL Mater. **3**, 041502 (2015).
[12] K. Kosuge, J. Phys. Soc. Japan **22**, 551 (1967).
[13] J. Cao, Y. Gu, W. Fan, L. Q. Chen, D. F. Ogletree, K. Chen, N. Tamura, M. Kunz, C. Barrett, J. Seidel, and J. Wu, Nano Lett. **10**, 2667 (2010).
[14] J. H. Park, J. M. Coy, T. S. Kasirga, C. Huang, Z. Fei, S. Hunter, and D. H. Cobden, Nature **500**, 431 (2013).
[15] J. P. Pouget, H. Launois, J. P. D'Haenens, P. Merenda, and T. M. Rice, Phys. Rev. Lett. **35**, 873 (1975).
[16] J. P. Pouget, H. Launois, T. M. Rice, P. Dernier, A. Gossard, G. Villeneuve, and P. Hagenmuller, Phys. Rev. B **10**, 1801 (1974).
[17] K. Okimura, T. Watanabe, and J. Sakai, J. Appl. Phys. **111**, 073514 (2012).
[18] A. Rúa, R. Cabrera, H. Coy, E. Merced, N. Sepúlveda, and F. E. Fernández, J. Appl. Phys. **111**, 104502 (2012).
[19] E. Strelcov, A. Tselev, I. Ivanov, J. D. Budai, J. Zhang, J. Z. Tischler, I. Kravchenko, S. V Kalinin, and A. Kolmakov, Nano Lett. **12**, 6198 (2012).
[20] E. Arcangeletti, L. Baldassarre, D. Di Castro, S. Lupi, L. Malavasi, C. Marini, A. Perucchi, and P. Postorino, Phys. Rev. Lett. **98**, 196406 (2007).
[21] J. Laverock, S. Kittiwatanakul, A. Zakharov, Y. Niu, B. Chen, S. A. Wolf, J. W. Lu, and K. E. Smith, Phys. Rev. Lett. **113**, 216401 (2014).
[22] T. Yao, X. Zhang, Z. Sun, S. Liu, Y. Huang, Y. Xie, C. Wu, X. Yuan, W. Zhang, Z. Wu, G. Pan, F. Hu, L. Wu, Q. Liu, and S. Wei, Phys. Rev. Lett. **105**, 226405 (2010).

[23] D. Wegkamp, M. Herzog, L. Xian, M. Gatti, P. Cudazzo, C. L. McGahan, R. E. Marvel, R. F. Haglund, A. Rubio, M. Wolf, and J. Stähler, Phys. Rev. Lett. **113**, 216401 (2014).
[24] V. R. Morrison, R. P. Chatelain, K. L. Tiwari, A. Hendaoui, A. Bruhacs, M. Chaker, and B. J. Siwick, Science (80-.). 346, 445 (2014).
[25] H.-T. Kim, Y. W. Lee, B.-J. Kim, B.-G. Chae, S. J. Yun, K.-Y. Kang, K.-J. Han, K.-J. Yee, and Y.-S. Lim, Phys. Rev. Lett. **97**, 266401 (2006).
[26] H.-T. Kim, B.-G. Chae, D.-H. Youn, S.-L. Maeng, G. Kim, K.-Y. Kang, and Y.-S. Lim, New J. Phys. **6**, 52 (2004).
[27] J. B. Goodenough, J. Solid State Chem. **3**, 490 (1971).
[28] A. Zylbersztejn and N. F. Mott, Phys. Rev. B **11**, 4383 (1975).
[29] R. M. Rice, H. Launois, and J. P. Pouget, Phys. Rev. Lett. **73**, 3042 (1994).
[30] R. M. Wentzcovitch, Phys. Rev. Lett. **72**, 3389 (1994).
[31] R. M. Wentzcovitch, W. W. Schulz, and P. B. Allen, Phys. Rev. Lett. **73**, 3043 (1994).
[32] S. Biermann, A. Poteryaev, A. I. Lichtenstein, and A. Georges, Phys. Rev. Lett. **94**, 026404 (2005).
[33] C. Weber, D. D. O'Regan, N. D. M. Hine, M. C. Payne, G. Kotliar, and P. B. Littlewood, Phys. Rev. Lett. **108**, 256402 (2012).
[34] M. Gatti, F. Bruneval, V. Olevano, and L. Reining, Phys. Rev. Lett. **99**, 266402 (2007).
[35] L. Hedin, Phys. Rev. **139**, A796 (1965).
[36] V. Eyert, Phys. Rev. Lett. **107**, 016401 (2011).
[37] X. Yuan, Y. Zhang, T. A. Abtew, P. Zhang, and W. Zhang, Phys. Rev. B **86**, 235103 (2012).
[38] R. Grau-Crespo, H. Wang, and U. Schwingenschlögl, Phys. Rev. B **86**, 081101 (2012).
[39] B. Xiao, J. Sun, A. Ruzsinszky, and J. P. Perdew, Phys. Rev. B **90**, 085134 (2014).
[40] H. Zheng and L. K. Wagner, Phys. Rev. Lett. **114**, 176401 (2015).
[41] K. Kosuge, Y. Ueda, S. Kachi, T. Shinjo, T. Takada, and M. Takano, J. Solid State Chem. **23**, 105 (1978).
[42] P. Pouget, P. Lederer, D. Schreiber, H. Launois, D. Wohlleben, A. Casalot, and G. Villeneuve, J. Phys. Chem. Solids **33**, 1961 (1972).
[43] G. Kresse and D. Joubert, Phys. Rev. B **59**, 1758 (1999).
[44] G. Kresse and J. Furthmüller, Phys. Rev. B **54**, 11169 (1996).
[45] J. P. Perdew, M. Ernzerhof, and K. Burke, J. Chem. Phys. **105**, 9982 (1996).
[46] C. Adamo and V. Barone, J. Chem. Phys. **110**, 6158 (1999).
[47] J. B. Goodenough, J. Phys. Chem. Solids **6**, 287 (1958).
[48] J. B. Goodenough, Phys. Rev. **100**, 564 (1955).
[49] J. Kanamori, J. Phys. Chem. Solids **10**, 87 (1959).
[50] J. M. Longo, P. Kierkegaard, C. J. Ballhausen, U. Ragnarsson, S. E. Rasmussen, E. Sunde, and N. A. Sørensen, Acta Chem. Scand. **24**, 420 (1970).
[51] D. B. McWhan, M. Marezio, J. P. Remeika, and P. D. Dernier, Phys. Rev. B **10**, 490 (1974).
[52] M. Marezio, D. B. McWhan, J. P. Remeika, and P. D. Dernier, Phys. Rev. B **5**, 2541 (1972).

[53] H. Wang, T. A. Mellan, R. Grau-Crespo, and U. Schwingenschlögl, Chem. Phys. Lett. **608**, 126 (2014).
[54] B. Xiao, J. Sun, A. Ruzsinszky, and J. P. Perdew, Phys. Rev. B **90**, 085134 (2014).
[55] T. C. Koethe, Z. Hu, M. W. Haverkort, C. Schüßler-Langeheine, F. Venturini, N. B. Brookes, O. Tjernberg, W. Reichelt, H. H. Hsieh, H. J. Lin, C. T. Chen, and L. H. Tjeng, Phys. Rev. Lett. **97**, 116402 (2006).
[56] R. Molaei, R. Bayati, S. Nori, D. Kumar, J. T. Prater, and J. Narayan, Appl. Phys. Lett. **103**, 252109 (2013).
[57] K. Schwarz, J. Phys. F Met. Phys. **16**, L211 (1986).
[58] I. I. Mazin, D. J. Singh, and C. Ambrosch-Draxl, Phys. Rev. B **59**, 411 (1999).
[59] H. Guo, K. Chen, Y. Oh, K. Wang, C. Dejoie, S. a Syed Asif, O. L. Warren, Z. W. Shan, J. Wu, and a M. Minor, Nano Lett. **11**, 3207 (2011).
[60] E. O. Wollan and W. C. Koehler, Phys. Rev. **100**, 545 (1955).
[61] K. Okimura, N. Hanis Azhan, T. Hajiri, S. Kimura, M. Zaghrioui, and J. Sakai, J. Appl. Phys. **115**, 153501 (2014).
[62] J. B. Goodenough and H. Y.-P. Hong, Phys. Rev. B **8**, 1323 (1973).
[63] M. Rohlfing and S. G. Louie, Phys. Rev. Lett. **81**, 2312 (1998).
[64] F. J. Nelson, J.-C. Idrobo, J. D. Fite, Z. L. Mišković, S. J. Pennycook, S. T. Pantelides, J. U. Lee, and A. C. Diebold, Nano Lett. **14**, 3827 (2014).
[65] M.A. Korotin, N. A. Skorikov, and V. I. Anisimov, Phys. Met. Met. **94**, 17 (2002).
[66] A. Liebsch, H. Ishida, and G. Bihlmayer, Phys. Rev. B **71**, 085109 (2005).

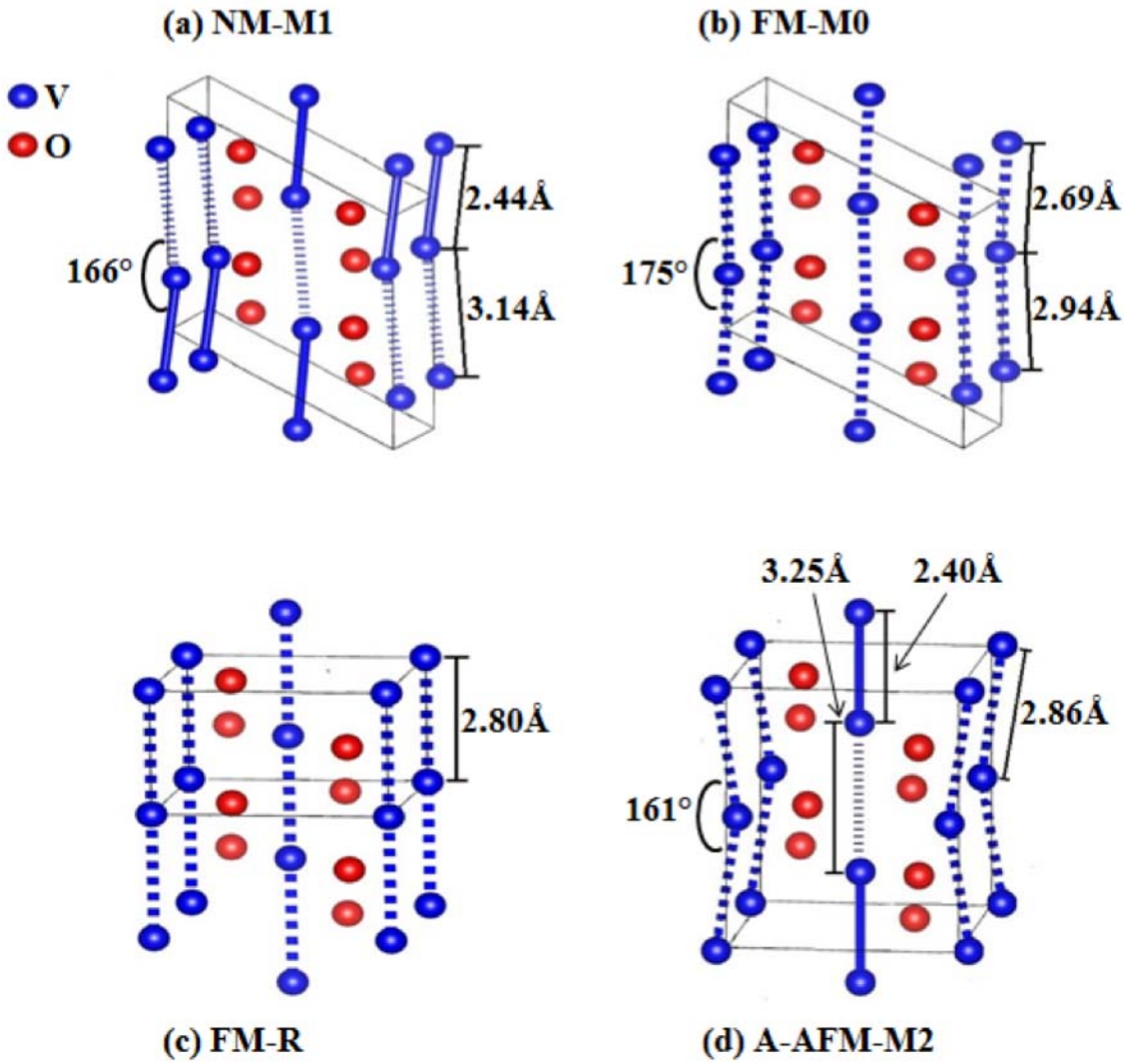

FIG. 1 (color online). Optimized structures of different VO_2 phases: (a) NM-M1, (b) FM-M0, (c) FM-R, and (d) A-AFM-M2. Short V-V bonds (<2.50Å) are shown as solid lines ( ) while long bonds (>3.00Å) have dotted lines ( ). V-V bonds with lengths between 2.50 and 3.00Å have dashed lines ( ).

TABLE I. Comparison of lattice constants, V-V bond lengths, and V-V bond angles from this work and experiment (Exp). Note that the FM-M0 state values are compared to the monoclinic metallic state (mM) values as determined from x ray absorption fine structure measurements.

		M1	NM-M1	mM	FM-M0	R		M2	
		Exp [50]	This work	Exp [22]	This work	Exp [51]	This work	Exp [52]	This work
a (Å)		5.75	5.53	5.69	5.59	4.55	4.42	9.07	8.98
b (Å)		4.54	4.51	4.59	4.50	4.55	4.42	5.80	5.65
c (Å)		5.38	5.28	5.29	5.29	2.85	2.80	4.53	4.48
α, γ (°)		90	90	90	90	90	90	90	90
β (°)		122.65	121.93	122.61	122.05	90	90	91.88	91.88
V-V bond (Å)	short	2.62	2.44	2.72	2.69	2.85	2.80	2.54	2.40
	middle							2.93	2.86
	long	3.17	3.14	2.98	2.94			3.26	3.25
V-V angle (°)		168	166		175	90	90	162	161

TABLE II. Calculated magnetic grounds states and band gaps of VO_2 phases compared to experiment.

		Experiment	Theoretical results					
			This work	HSE			GW	DMFT
				[36] [c]	[38] [d]	[37]	[34]	[32] [g]
Magnetic ground states	M0	FM/PM [41,42] [a]	FM					
	M1	NM [11,56] [b]	NM		AFM	AFM		
	M2	AFM [16]	A-AFM			FM		
Band gap (eV)	M1	0.6-0.7 [9,10]	0.63	1.10	2.23 (AFM) 0.98 (NM) [e]		0.65	0.60
	M2	>0.10 [61]	0.56	1.20				
	R	0 [9,10]	0	0	1.43 (FM) 0 (NM) [f]		0	0

[a] Divergence of the magnetic susceptibility below 30 K underlines the importance of exploring the unknown low-temperature magnetic properties.

[b] The disagreement of measurements of small positive [11] susceptibility and another publication [56] reporting small negative susceptibility justified our designation of M1 as NM as similar to previous authors [38].

[c] Band gap of each VO_2 phase was calculated by assuming the magnetic state found in experiments.

[d] Non-spin-polarized calculations similar to those of Eyert [36] were reproduced and then spin-polarized calculations for each potential magnetic state were performed [38].

[e] The correct magnetic phase, NM-M1, has a calculated band gap is close to the experimental value. However, AFM-M1 was calculated to be lower in energy, and the band gap is over thrice the expected value.

[f] A ferromagnetic R state with a band gap of 1.43 eV was calculated to be the ground state. However, a NM state with a correct band gap of 0 was also obtained, albeit at a higher energy.

[g] A stable nonmagnetic structure was obtained with cluster-DMFT, but it was not compared to other magnetic states to determine the ground state.

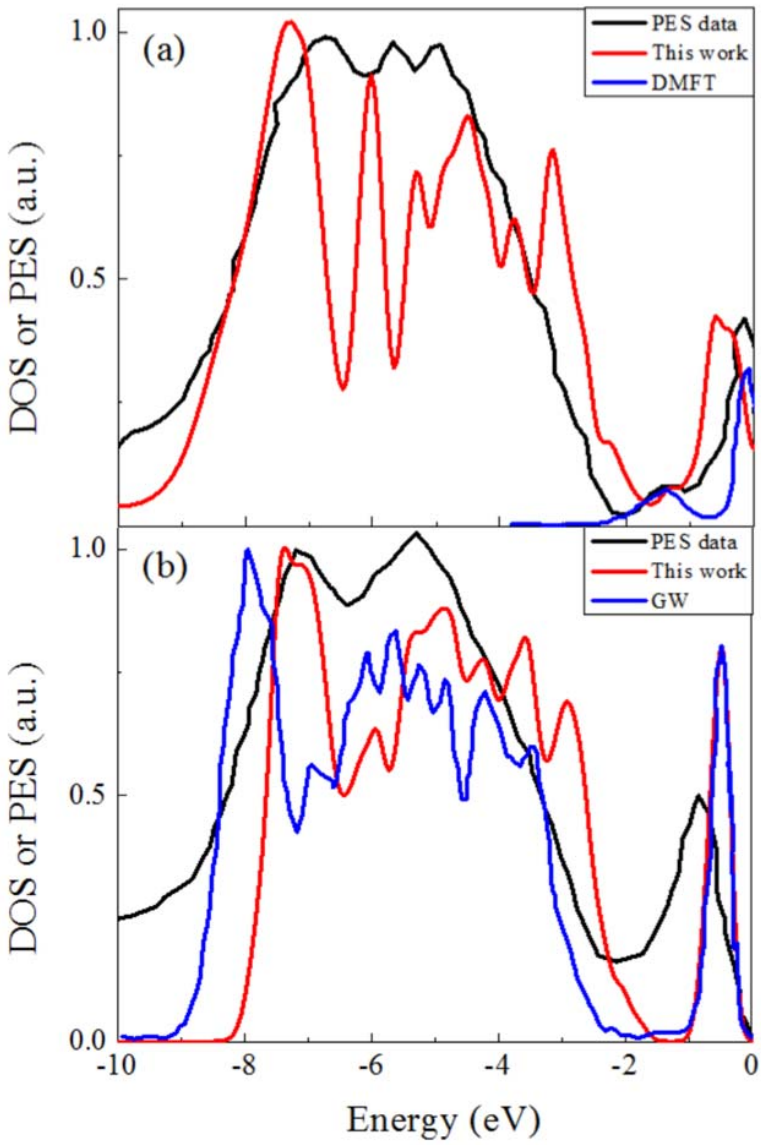

FIG. 2 (color online). (a) The DOS of FM-R calculated in this work (red) is compared with the experimental [55] photoemission spectrum (black) and the V 3d (t_{2g}) spectral weights (blue) from LDA+DMFT calculations [32]. The 1.3 eV satellite feature is clearly found in this work. (b) The total DOS of NM-M1 calculated in this work (red) is compared with the experimental [55] photoemission spectrum (black) of the low temperature insulating M1 and the DOS (blue) from GW calculations [34]. Each DOS from this work was convoluted with a Gaussian function.

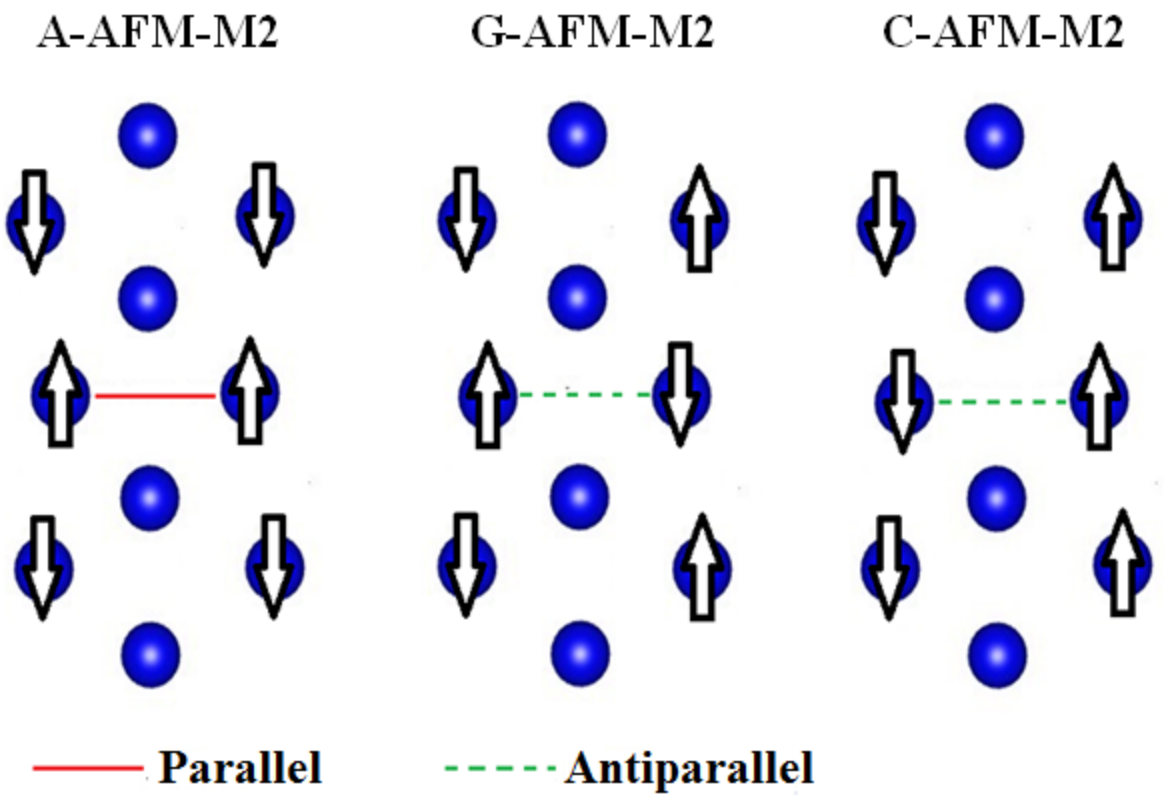

FIG. 3 (color online). Schematic of the three possible magnetic structures of AFM-M2: A-AFM, G-AFM and C-AFM. The blue solid circles are V atoms and the white arrows represent their magnetic moments. The solid line between two adjacent canted chains represents parallel magnetic moments between the nearest vanadium atoms from each chain, while the dashed lines represent an antiparallel configuration. The A-AFM configuration has the lowest energy.